Global Phase Diagram of the Normal State of Twisted Bilayer Graphene

Glenn Wagner[1,2] Yves H. Kwan[1] Nick Bultinck[1,3] Steven H. Simon[1] and S. A. Parameswaran[1]
[1]Rudolf Peierls Centre for Theoretical Physics, Parks Road, Oxford OX1 3PU, United Kingdom
[2]Department of Physics, University of Zurich, Winterthurerstrasse 190, 8057 Zurich, Switzerland
[3]Department of Physics, Ghent University, Krijgslaan 281, 9000 Gent, Belgium

(Received 7 October 2021; accepted 28 March 2022; published 12 April 2022)

We investigate the full doping and strain-dependent phase diagram of the normal state of magic-angle twisted bilayer graphene (TBG). Using comprehensive Hartree-Fock calculations, we show that at temperatures where superconductivity is absent the global phase structure can be understood based on the competition and coexistence between three types of intertwined orders: a fully symmetric phase, spatially uniform flavor-symmetry-breaking states, and an incommensurate Kekulé spiral (IKS) order. For small strain, the IKS phase, recently proposed as a candidate order at all nonzero integer fillings of the moiré unit cell, is found to be ubiquitous for noninteger doping as well. We demonstrate that the corresponding electronic compressibility and Fermi surface structure are consistent with the "cascade" physics and Landau fans observed experimentally. This suggests a unified picture of the phase diagram of TBG in terms of IKS order.

DOI: 10.1103/PhysRevLett.128.156401

Introduction.—When two layers of graphene are stacked with a relative twist close to the "magic angle" ($\sim 1^\circ$) the resulting moiré pattern leads to a band structure with very flat bands, enhancing correlation effects [1]. As the number of electrons per moiré unit cell (i.e., the filling ν, measured relative to neutrality) is varied, twisted bilayer graphene (TBG) exhibits a rich array of insulating, metallic, semimetallic, topological, and superconducting behavior [2–7]. Much theoretical effort has been expended in attempts to formulate a consistent framework explaining these phenomena [8–41]. Three main classes of experimental data (detailed below) guide such a framework: (zero-field) transport measurements, compressibility measurements (cascades), and Landau fan diagrams. In this Letter we use microscopic Hartree-Fock (HF) calculations, which crucially incorporate strain and allow for spatially modulated order, to establish a global normal state phase diagram of TBG that is consistent with all these experimental results.

Transport measurements above T_c reveal a semimetal [3–5,42–50] or insulator [2,6,7,51–55] at $\nu = 0$, a metal or weak insulator at $\nu = \pm 1$, correlated insulators at $\nu = \pm 2$ [2,3,5–7,42–55] and ± 3 [2,5–7,44,46,47,49,51–55], and metallic behavior [2–7,42–55] at all noninteger fillings. Strong-coupling calculations predict an insulator at $\nu = 0$ [11,21]; thus the observed semimetallic behavior indicates that experimental TBG samples lie outside the strong coupling regime. Theoretically, it has been demonstrated that even small amounts of strain suppress strong coupling insulators at $\nu = 0$ [36] in favor of semimetallic behavior. Since finite heterostrain of strength $\epsilon = 0.1$–0.7% has been measured via scanning probes [56–59] in many TBG samples and is likely ubiquitous, its inclusion provides a compelling explanation of experiments at charge neutrality.

Viewing strain as a key ingredient at $\nu = 0$ profoundly impacts the understanding of TBG at other commensurate fillings. In recent work we and others [25] argued that a new state, dubbed the incommensurate Kekulé spiral (IKS), emerges at all nonzero integer fillings in the range of modest strain invoked to explain the $\nu = 0$ semimetal. Via HF analysis, we identified IKS order as an energetically favored and experimentally consistent candidate for the metallic states at $\nu = \pm 1$ and the gapped insulators at $\nu = \pm 2, \pm 3$. Here, we explore the relationship between the physics at noninteger ν and the previously identified states at integer ν.

A stringent test for theory is to reproduce the phenomenology of the Fermi surfaces (FSs) that emerge on doping away from commensuration. One such feature is "cascade physics": the sequence of density-tuned transitions which repeats roughly each time ν is increased by one. Scanning tunneling experiments [59–61] show distinct changes in the excitation spectrum at each integer filling, whereas compressibility measurements show a characteristic repeating sawtooth pattern in the chemical potential μ [42,45,49,50,53,62,63]: As ν approaches each positive integer from below, μ increases sharply, before gradually decreasing towards the next integer ν. A complementary perspective is given by the "Landau fans" of field-dependent densities where the longitudinal magnetoresistivity $\rho_{xx}(B)$ reaches a minimum, corresponding to filled Landau levels. These reveal the number of degenerate FSs that emerge from the commensurate fillings. On the electron-doped side of $\nu = 0$, 2, 3, experiments find

4,2,1 FSs, respectively [2–7,42,45–47,49,51,52,64]. Hole-doping negative integers yields analogous scenarios due to approximate particle-hole symmetry [65].

The flavor degeneracy of TBG is crucial to understanding cascade physics. Focusing on the two flat central bands, there are four flavors of electrons (two spins and two valleys) so that 8 electrons per moiré unit cell are necessary to completely fill the TBG flat bands. Empirically, flavor-symmetry breaking transitions occur near van Hove singularities between integer fillings [9], with the density of electrons in partially filled bands resetting to zero at each integer; however, the mechanism behind the cascades remains controversial. Although both weak- and strong-coupling approaches invoke the competition between Coulomb exchange (which favors flavor polarization) and kinetic energy (minimized by equal flavor populations), they differ in details. Weak-coupling theories build on the bare dispersion [45] and its linearity near Dirac points; since each flavor has two Dirac cones near K_M, K'_M in the moiré Brillouin zone (mBZ), in this "Dirac cascade" picture the sequence of electron-doped FSs is 8, 6, 4, 2, inconsistent with measured Landau fans unless, e.g., C_3 symmetry is broken [67]. In contrast, strong-coupling treatments rely on the renormalization of the bare band structure by interactions: within HF the Dirac cones are replaced by a large correlation dip, i.e., a minimum in the dispersion, near Γ_M [53,68–72]. On doping, this yields a single FS per flavor and hence gives Landau fans consistent with experiment [72].

Despite such successes, a strong-coupling calculation that ignores corrections from the single-particle dispersion fails other tests. Notably, it ignores strain, which is essential to reproduce the $\nu = 0$ semimetal as well as the metallic behavior at $\nu = \pm 1$ seen by many experiments. Even for zero strain, in a strong-coupling calculation it is necessary to include a small amount of kinetic energy in order to pick out the Kramers intervalley coherent (KIVC) insulator (known to be the unstrained HF ground state at $\nu = 0, \pm 2$ for realistic interactions [11,21]) from a degenerate manifold of flavor-symmetry-broken states. In the presence of an experimentally realistic amount of strain, the kinetic energy is further enhanced, hence requiring an intermediate-coupling analysis, as used in Ref. [25] to argue that IKS order consistently explains metallic and insulating behavior at different integer ν. A natural question is whether this approach also reproduces the cascade physics and Landau fan degeneracies.

With this motivation, we extend the study of TBG with strain [25,36] to the gapless states at non-integer fillings of the central bands. We demonstrate numerically that finite-strain IKS order remains stable when the system is doped away from integer filling, and analyze the Fermi surfaces and the chemical potential variation over the full range of experimentally relevant fillings and strains. We find that the electronic compressibility matches experiment reasonably well for *all* strains, even though the phase structure changes significantly for $\epsilon \gtrsim 0.2\%$, suggesting that cascade physics places far weaker constraints on theory than previously assumed. We argue therefore that Landau fan degeneracy and the absence or presence of insulating states at integer fillings are more informative diagnostics of the underlying physics. Strain and the resulting IKS order are vital for the HF calculation to agree with both experimental probes. The ubiquity of IKS order at almost all fillings for the relevant strains suggests this is the universal normal state of TBG from which superconductivity emerges at low temperatures.

Results.—We perform self-consistent HF calculations of the interacting Bistritzer-Macdonald (BM) model [1] projected to the central bands and without substrate potential or nonlocal tunneling. We use hopping parameters $w_{AA} = 82.5$ meV and $w_{AB} = 110$ meV and work at a twist angle of $\theta = 1.1°$. We include heterostrain of strength ϵ and axis along $\hat{\mathbf{x}}$ using the prescription of Refs. [25,36,73]. We verified that variations in twist angle and strain axis do not qualitatively change the phase diagram. The Hamiltonian has approximate particle-hole symmetry, allowing us to restrict discussion to positive ν [65]. We use the dual-gate screened Coulomb interaction $V(q) = (e^2/2\epsilon_0\epsilon_r q)\tanh qd$ with screening length $d = 25$ nm and relative permittivity $\epsilon_r = 10$. To avoid double-counting interactions, we subtract off a density matrix corresponding to decoupled graphene layers at charge neutrality [10,11]. We show that other subtraction schemes lead to similar results (See Supplemental Material [65]). Further HF details are in Ref. [25].

Diagonalizing the sublattice operator (ignoring the weak dispersion) defines the "Chern basis" $\hat{c}^\dagger_{\mathbf{k},\tau s\sigma}$ for the eight central bands [11], which can then be labelled by valley, spin, and sublattice polarization (with Pauli matrices τ_μ, s_μ, and σ_μ, respectively), with the Chern number of each band given by $C = \sigma_z\tau_z$. In the strong coupling limit, the integer-filling ground states are uniform ferromagnets in this basis, in analogy with quantum Hall ferromagnetism (QHFM) [11,21]. However, on including finite strain the system leaves the strong coupling limit, and hosts new phases: A fully-symmetric phase and the IKS order. All these orders can be captured by the one-particle density matrix

$$\langle \hat{c}^\dagger_{\mathbf{k}-\tau\mathbf{q}/2,\tau s\sigma}\hat{c}_{\mathbf{k}-\tau'\mathbf{q}/2,\tau' s'\sigma'}\rangle = P_{\tau s\sigma;\tau' s'\sigma'}(\mathbf{k}), \tag{1}$$

with $\mathrm{Tr}P = (\nu + 4)N_1N_2$, where $N = N_1N_2$ is the number of moiré unit cells. We have shifted the momenta such that we always hybridize electrons with momentum $\mathbf{k} - \tau\mathbf{q}/2$ in valley τ with electrons with momentum $\mathbf{k} - \tau'\mathbf{q}/2$ in valley τ'. That way intravalley ($\tau = \tau'$) hybridization occurs at equal momenta while intervalley ($\tau \neq \tau'$) coherence (IVC) occurs with relative momentum $\mathbf{q}$. We choose the HF solution with the lowest energy for any $\mathbf{q}$ in the mBZ. We find two types of IVC states: Kramers-IVC (KIVC) order [11] at $\mathbf{q} = 0$ and time-reversal symmetric $\mathcal{T}$IVC

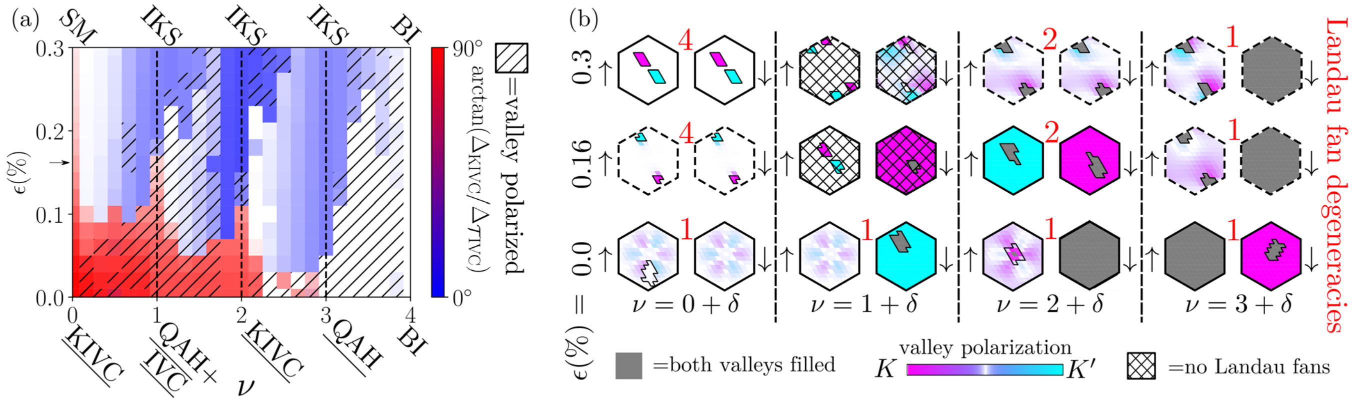

FIG. 1. (a) Hartree-Fock phase diagram of TBG in the filling-strain plane. Color map intensity shows the magnitude of the IVC order parameter (white regions have no IVC). Color encodes type of IVC via the angle $\arctan(\Delta_{\mathrm{KIVC}}/\Delta_{\mathcal{T}\mathrm{IVC}})$ on the "Bloch sphere," KIVC at $\mathbf{q}=0$ (red) and $\mathcal{T}$IVC at nonzero $\mathbf{q}$ (blue). Hatching denotes valley polarization. $\mathcal{T}$-breaking phases are underlined. HF results are for 12×12 systems, minimizing over all $\mathbf{q}$. (b) Electron-doped FSs (black lines) of both spin species $(\uparrow,\downarrow)$ near commensurate filling at three representative strains. In IVC phases, valleys hybridize as indicated by the modulated valley polarization, yielding two split bands of which only the lower is shown. Finite-$\mathbf{q}$ IVC order is flagged by dashed mBZ boundaries ($\mathbf{q}$ may vary). Experimentally measured Landau fans indicate 4,2,1 equal-area FSs on electron-doping $\nu=0$, 2, 3. HF results at $\epsilon=0.16\%$ and $\epsilon=0.3\%$ are consistent with this, but not at $\epsilon=0$, suggesting strain is ubiquitous in real samples. Metallic parent states at $\nu=1$, $\epsilon=0.16\%, 0.3\%$ (hatched) do not give rise to clear Landau fans, consistent with experiments.

order at variable $\mathbf{q}\neq 0$ (this is the so-called IKS order [25]). We can define the spinless time-reversal symmetry $\mathcal{T}=\tau_x\mathcal{K}$ and the related antiunitary symmetry $\mathcal{T}'=\tau_y\mathcal{K}$, where $\mathcal{K}$ denotes complex conjugation. The KIVC order parameter $\Delta_{\mathrm{KIVC}}=\tau_{x,y}\sigma_y$ then satisfies $\mathcal{T}'$ whereas $\mathcal{T}$IVC with $\Delta_{\mathcal{T}\mathrm{IVC}}=\tau_{x,y}\sigma_x$ respects $\mathcal{T}$.

Figure 1(a) shows a global phase diagram of TBG in the filling-strain plane. We find the different types of order listed in Table I. Between $\nu=0$ and $\nu=2$ we find KIVC order at $\mathbf{q}=0$ for small strains (red regions). As noted, this is known to be the zero-strain HF ground state at $\nu=0$ and $\nu=2$. At $\nu=0$ the ground state switches from the insulating KIVC to a semimetallic state (SM) at a critical value of strain (larger than $\epsilon=0.3\%$ for the chosen parameters), as previously reported [36]. This semimetal persists to finite doping as a symmetric metal (white region). For modest values of strain and mostly on the hole-doped side of the integers, we find IKS order at finite $\mathbf{q}$ (blue regions) that was previously reported only at integer fillings [25]. Finally, there are other generalized ferromagnets besides the KIVC: quantized anomalous Hall (QAH), valley polarized (VP), valley Hall (VH), and spin Hall (SH) [74] states (white regions) that are in close energetic competition with the IKS solution. Between the integer fillings, we find first-order phase transitions where the ground state crosses over between an IKS solution and a VP solution (between $\nu=1$–2 and $\nu=3$–4) or a VH/SH solution (between $\nu=2$–3; the two solutions are degenerate in our calculation, however intervalley Hund's coupling favors the VH state [65]). VP can also coexist with the KIVC and IKS away from the integer fillings. $\mathcal{T}$ breaking is ubiquitous at zero strain, but is almost completely absent for $\epsilon=0.3\%$.

We have verified that the order parameters remain nonzero in finite-temperature HF for temperatures up to ~50 K [65], although those that break $U(1)$ symmetries

TABLE I. Order parameters and representative projectors P in the Chern basis at a given reference ν. Doped versions of these phases appear at noninteger fillings. Asterisks denote degenerate manifolds of states with different spin polarizations obtained by performing valley-dependent spin rotations allowed by $\mathrm{SU}(2)_K\times\mathrm{SU}(2)_{K'}$ symmetry. $\boldsymbol{\gamma}=(\sigma_x,\tau_z\sigma_y,\tau_z\sigma_z)$, $\boldsymbol{\eta}=(\tau_x\sigma_x,\tau_y\sigma_x,\tau_z)$ and $\mathbf{n_k}$, $\mathbf{m_k}$ are three-vectors ($\mathbf{n_k}$ lies in the x-y plane).

Phase	Ref. ν	Spin pol.	Valley pol.	$U(1)_V$	$\hat{\mathcal{T}}=\tau_x\hat{\mathcal{K}}$	$\hat{\mathcal{T}}'=\tau_y\hat{\mathcal{K}}$	$P=\langle\hat{c}^{\dagger}_{\mathbf{k},\tau s\sigma}\hat{c}_{\mathbf{k}',\tau's'\sigma'}\rangle$
IKS	−3	*	0	✗	✓	✗	$\frac{1}{8}(1+s_z)(1+\mathbf{n_k}\cdot\boldsymbol{\gamma})(\delta_{\mathbf{k},\mathbf{k}'}+\mathbf{m}^{\perp}_{\mathbf{k}}\cdot\boldsymbol{\eta}^{\perp}\delta_{\mathbf{k},\mathbf{k}'+q}+m^z_{\mathbf{k}}\eta^z\delta_{\mathbf{k},\mathbf{k}'})$
VP	−2	2	2	✓	✗	✗	$\frac{1}{4}(1+s_z)(1+\tau_z)\sigma_0\delta_{\mathbf{k},\mathbf{k}'}$
SH	−2	0	2	✓	✗	✗	$\frac{1}{4}(1+\tau_z)(1+\sigma_z s_z)\delta_{\mathbf{k},\mathbf{k}'}$
VH	−2	*	0	✓	✓	✓	$\frac{1}{4}\tau_0(1+s_z)(1+\sigma_z)\delta_{\mathbf{k},\mathbf{k}'}$
QAH	−3	1	1	✓	✗	✗	$\frac{1}{8}(1+s_z)(1+\sigma_z)(1+\tau_z)\delta_{\mathbf{k},\mathbf{k}'}$
KIVC	−2	*	0	✗	✗	✓	$\frac{1}{4}(1+s_z)[1+(\cos\theta_{\mathrm{IVC}}\tau_x+\sin\theta_{\mathrm{IVC}}\tau_y)\sigma_y]\delta_{\mathbf{k},\mathbf{k}'}$

will only have algebraic correlations once fluctuations beyond mean field are included. Consequently, the phases studied here are possible parent states for the superconductors that emerge in experiments below $T_c \lesssim 5$ K [2–5].

Depending on the strain, different pictures emerge for the cascades. At zero strain, at $\nu = 0$ the system begins in KIVC, with IVC in both spin species. Upon doping, down spins continue to have IVC order, while up spins valley polarize. At $\nu = 1$, down spins are in a KIVC insulator while up spins form a QAH state. We move to $\nu = 2$ by doping up spins until they are fully filled, while down spins are in KIVC. Doping beyond $\nu = 2$, KIVC order is destroyed in the down spins, which now become valley polarized and eventually form QAH state at $\nu = 3$.

At finite strain, doping the semimetal at neutrality gives four FSs from the two spins and two valleys. The states are filled from the Hartree minima, which shift away from Γ_M by equal and opposite amounts in each valley, consistent with C_2 symmetry. At a critical filling, the Fermi seas of the two valleys start overlapping, signaling the onset of finite-**q** IVC order (IKS). By the time the next integer filling is reached, the IKS order has proliferated throughout the mBZ (except near the Hartree minima, where electrons remain valley polarized). Therefore we can view the emergence of IKS order at critical fillings as a weak-coupling instability of a FS from interaction-renormalized bands. For $\epsilon =$ 0.1–0.2% there are regions on the electron-doped sides of $\nu = 0$, 1, 2, 3 where the ground state lacks any IVC order. By counting the number of (equal area) FSs [Fig. 1(b)] we obtain Landau fan degeneracies of 4,2,1 at $\nu = 0$, 2, 3, respectively. For larger strains the ground state always includes some IKS order (except for fillings close to $\nu = 0$, 4) with wave vector **q** whose optimal value varies throughout the mBZ as the filling changes (see Supplemental Material [65] for ϵ and ν dependence of **q**). For the "Kekulé cascades", the Landau fan degeneracies at $\nu = 0$, 2, 3 are 4,2,1, respectively. Since we find a metal at $\nu = 1$, no clear Landau fans would emanate from this filling, consistent with all experiments under normal conditions [2,4,5,46,47]. A striking feature seen in experiments is the asymmetry of the Landau fans: At $\nu = \pm 2, \pm 3$, the Landau fans are only seen for doping away from charge neutrality [2–7,42,45–47,49,51,52,64]. By calculating the density of states at the Fermi surface, we see that for doping towards charge neutrality the bands are very flat and there is no sharp Fermi surface consistent with the absence of Landau fans. We see this phenomenology for any value of the strain (see Supplemental Material [65]).

The traces of the chemical potential in Fig. 2 show a sawtooth pattern that is consistent with the experimental observations reported in Refs. [42,45]. The phases on the hole-doped side of integer filling are more compressible than those on the electron-doped side. For larger strains, the chemical potential is a smoother function of filling closer to the "square root" shape previously thought to be a unique signature of an underlying Dirac description [45]. To understand this, note that at the largest values of the strain (~0.3%) there is a continuous range of IKS. The IKS state evolves smoothly, with a gradually changing **q**, leading to a smooth variation in the chemical potential (up to finite-size effects). Furthermore, the chemical potential increases by 40 meV between $\nu = 0$ and $\nu = 4$, consistent with Refs. [42,45,59,62,72]. We note, however, that the chemical potential traces are relatively insensitive to the underlying phases, and the resetting of the chemical potential at integer fillings is a generic feature both of our HF studies at *all* strains and also of zero-strain calculations at both weak [45] and strong [72] coupling. In contrast, Landau fans are sensitive to the number and structure of the FSs and are hence better able to distinguish between competing scenarios.

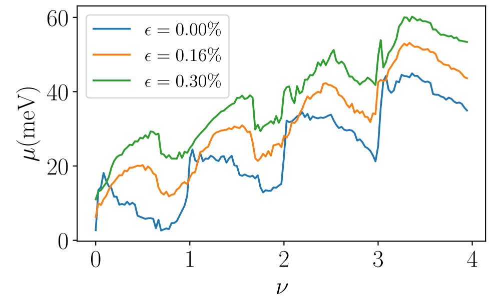

FIG. 2. Chemical potential μ as a function of filling ν for three different strain values, offset by 5 meV for clarity. HF calculation for a 12×12 system with steps of $\Delta\nu = 1/36$.

Conclusions.—In this work we have fleshed out the full HF phase diagram of TBG above T_c for any filling ν of the central bands and and as a function of strain ϵ, and demonstrated that it captures key experimental features of TBG (modulo superconductivity). Reproducing the correct Landau fans and semimetallicity at $\nu = 0$ requires an intermediate coupling picture with nonzero strain. A weak coupling description fails to reproduce the observed Landau fans, since the two Dirac points per noninteracting band doubles the number of Fermi surfaces relative to experiment. Absent strain, a strong coupling approach can reproduce the correct Landau fans, but predicts a gapped state at $\nu = 0$. This justifies our inclusion of both strain and realistic interactions as a necessary prerequisite to fully match experiments.

One of our key messages is that the normal state phase diagram of TBG can be understood in terms of three types of competing states: A symmetry-preserving metal and two classes of symmetry-breaking orders—IKS and a set of generalized ferromagnets. Without strain, the generalized ferromagnetic states are exact ground states [21] at integer fillings in an idealized limit of the Hamiltonian. In accord with this, we find that these states and their doped descendants describe the entire range of fillings at zero strain. However, strain is ubiquitous in experimental samples and upon its inclusion realistic TBG departs from the limit where generalized ferromagnets are ground states. This leads to the two types of states we find that do not lie within the manifold of generalized ferromagnets: The completely symmetric metal and the IKS state. For relatively modest strains of $\epsilon \gtrsim 0.3\%$, IKS order exists for almost the entire range of fillings ν. Because of its variable wave vector $\mathbf{q}$, the IKS order readily adjusts to changes in parameters, explaining its ubiquity in the phase diagram. This underscores the importance of an experimental search for this order. Furthermore, our study suggests that a doped IKS state could play the role of a parent to the superconducting order that emerges below T_c. The angle of the optimal IKS wave vector $\mathbf{q}$ varies as a function of filling [65], potentially providing an explanation for the rotating nematicity observed near T_c [43]. A theoretical investigation of a superconducting mechanism from an IKS parent state is clearly warranted, and may provide the final piece of the puzzle of competing orders in TBG.

This research was partially supported by the NCCR MARVEL, a National Centre of Competence in Research, funded by the Swiss National Science Foundation (Grant No. 182892). N. B. is supported by a senior postdoctoral research fellowship of the Flanders Research Foundation (FWO). We acknowledge support from the European Research Council under the European Union Horizon 2020 Research and Innovation Programme, Grant Agreement No. 804213-TMCS and from EPSRC Grant No. EP/S020527/1. Statement of compliance with EPSRC policy framework on research data: This publication is theoretical work that does not require supporting research data.

[1] R. Bistritzer and A. H. MacDonald, Moiré bands in twisted double-layer graphene, Proc. Natl. Acad. Sci. U.S.A. **108**, 12233 (2011).

[2] X. Lu, P. Stepanov, W. Yang, M. Xie, M. A. Aamir, I. Das, C. Urgell, K. Watanabe, T. Taniguchi, G. Zhang, A. Bachtold, A. H. MacDonald, and D. K. Efetov, Superconductors, orbital magnets and correlated states in magic-angle bilayer graphene, Nature (London) **574**, 653 (2019).

[3] Y. Cao, V. Fatemi, A. Demir, S. Fang, S. L. Tomarken, J. Y. Luo, J. D. Sanchez-Yamagishi, K. Watanabe, T. Taniguchi, E. Kaxiras, R. C. Ashoori, and P. Jarillo-Herrero, Correlated insulator behaviour at half-filling in magic-angle graphene superlattices, Nature (London) **556**, 80 (2018).

[4] Y. Cao, V. Fatemi, S. Fang, K. Watanabe, T. Taniguchi, E. Kaxiras, and P. Jarillo-Herrero, Unconventional superconductivity in magic-angle graphene superlattices, Nature (London) **556**, 43 (2018).

[5] M. Yankowitz, S. Chen, H. Polshyn, Y. Zhang, K. Watanabe, T. Taniguchi, D. Graf, A. F. Young, and C. R. Dean, Tuning superconductivity in twisted bilayer graphene, Science **363**, 1059 (2019).

[6] A. L. Sharpe, E. J. Fox, A. W. Barnard, J. Finney, K. Watanabe, T. Taniguchi, M. A. Kastner, and D. Goldhaber-Gordon, Emergent ferromagnetism near three-quarters filling in twisted bilayer graphene, Science **365**, 605 (2019).

[7] M. Serlin, C. L. Tschirhart, H. Polshyn, Y. Zhang, J. Zhu, K. Watanabe, T. Taniguchi, L. Balents, and A. F. Young, Intrinsic quantized anomalous Hall effect in a moiré heterostructure, Science **367**, 900 (2020).

[8] H. C. Po, L. Zou, A. Vishwanath, and T. Senthil, Origin of Mott Insulating Behavior and Superconductivity in Twisted Bilayer Graphene, Phys. Rev. X **8**, 031089 (2018).

[9] M. Xie and A. H. MacDonald, Weak-Field Hall Resistivity and Spin-Valley Flavor Symmetry Breaking in Magic-Angle Twisted Bilayer Graphene, Phys. Rev. Lett. **127**, 196401 (2021).

[10] M. Xie and A. H. MacDonald, Nature of the Correlated Insulator States in Twisted Bilayer Graphene, Phys. Rev. Lett. **124**, 097601 (2020).

[11] N. Bultinck, E. Khalaf, S. Liu, S. Chatterjee, A. Vishwanath, and M. P. Zaletel, Ground State and Hidden Symmetry of Magic-Angle Graphene at Even Integer Filling, Phys. Rev. X **10**, 031034 (2020).

[12] J. Liu and X. Dai, Theories for the correlated insulating states and quantum anomalous hall effect phenomena in twisted bilayer graphene, Phys. Rev. B **103**, 035427 (2021).

[13] T. Cea and F. Guinea, Band structure and insulating states driven by coulomb interaction in twisted bilayer graphene, Phys. Rev. B **102**, 045107 (2020).

[14] Y. Zhang, K. Jiang, Z. Wang, and F. Zhang, Correlated insulating phases of twisted bilayer graphene at commensurate filling fractions: A Hartree-Fock study, Phys. Rev. B **102**, 035136 (2020).

[15] M. Ochi, M. Koshino, and K. Kuroki, Possible correlated insulating states in magic-angle twisted bilayer graphene under strongly competing interactions, Phys. Rev. B **98**, 081102(R) (2018).

[16] J. Kang and O. Vafek, Strong Coupling Phases of Partially Filled Twisted Bilayer Graphene Narrow Bands, Phys. Rev. Lett. **122**, 246401 (2019).

[17] J. Kang and O. Vafek, Non-Abelian Dirac node braiding and near-degeneracy of correlated phases at odd integer filling in magic-angle twisted bilayer graphene, Phys. Rev. B **102**, 035161 (2020).

[18] O. Vafek and J. Kang, Renormalization Group Study of Hidden Symmetry in Twisted Bilayer Graphene with Coulomb Interactions, Phys. Rev. Lett. **125**, 257602 (2020).

[19] S. Liu, E. Khalaf, J. Y. Lee, and A. Vishwanath, Nematic topological semimetal and insulator in magic-angle bilayer graphene at charge neutrality, Phys. Rev. Research **3**, 013033 (2021).

[20] J. F. Dodaro, S. A. Kivelson, Y. Schattner, X. Q. Sun, and C. Wang, Phases of a phenomenological model of twisted bilayer graphene, Phys. Rev. B **98**, 075154 (2018).

[21] B. Lian, Z.-D. Song, N. Regnault, D. K. Efetov, A. Yazdani, and B. A. Bernevig, Twisted bilayer graphene. IV. Exact insulator ground states and phase diagram, Phys. Rev. B **103**, 205414 (2021).

[22] B. A. Bernevig, B. Lian, A. Cowsik, F. Xie, N. Regnault, and Z.-D. Song, Twisted bilayer graphene. v. exact analytic

many-body excitations in Coulomb Hamiltonians: Charge gap, Goldstone modes, and absence of Cooper pairing, Phys. Rev. B **103**, 205415 (2021).
[23] F. Xie, A. Cowsik, Z.-D. Song, B. Lian, B. A. Bernevig, and N. Regnault, Twisted bilayer graphene. VI. An exact diagonalization study at nonzero integer filling, Phys. Rev. B **103**, 205416 (2021).
[24] T. Soejima, D. E. Parker, N. Bultinck, J. Hauschild, and M. P. Zaletel, Efficient simulation of moiré materials using the density matrix renormalization group, Phys. Rev. B **102**, 205111 (2020).
[25] Y. H. Kwan, G. Wagner, T. Soejima, M. P. Zaletel, S. H. Simon, S. A. Parameswaran, and N. Bultinck, Kekulé Spiral Order at All Nonzero Integer Fillings in Twisted Bilayer Graphene, Phys. Rev. X **11**, 041063 (2021).
[26] P. Potasz, M. Xie, and A. H. MacDonald, Exact Diagonalization for Magic-Angle Twisted Bilayer Graphene, Phys. Rev. Lett. **127**, 147203 (2021).
[27] X. Zhang, G. Pan, Y. Zhang, J. Kang, and Z. Y. Meng, Momentum space quantum Monte Carlo on twisted bilayer graphene, Chin. Phys. Lett. **38**, 077305 (2021).
[28] L. Klebl, Z. A. H. Goodwin, A. A. Mostofi, D. M. Kennes, and J. Lischner, Importance of long-ranged electron-electron interactions for the magnetic phase diagram of twisted bilayer graphene, Phys. Rev. B **103**, 195127 (2021).
[29] G. Shavit, E. Berg, A. Stern, and Y. Oreg, Theory of Correlated Insulators and Superconductivity in Twisted Bilayer Graphene, Phys. Rev. Lett. **127**, 247703 (2021).
[30] F. Wu, A. H. MacDonald, and I. Martin, Theory of Phonon-Mediated Superconductivity in Twisted Bilayer Graphene, Phys. Rev. Lett. **121**, 257001 (2018).
[31] B. Lian, Z. Wang, and B. A. Bernevig, Twisted Bilayer Graphene: A Phonon-Driven Superconductor, Phys. Rev. Lett. **122**, 257002 (2019).
[32] F. Wu, E. Hwang, and S. Das Sarma, Phonon-induced giant linear-in-*t* resistivity in magic angle twisted bilayer graphene: Ordinary strangeness and exotic superconductivity, Phys. Rev. B **99**, 165112 (2019).
[33] C. Lewandowski, D. Chowdhury, and J. Ruhman, Pairing in magic-angle twisted bilayer graphene: Role of phonon and plasmon umklapp, Phys. Rev. B **103**, 235401 (2021).
[34] N. Bultinck, S. Chatterjee, and M. P. Zaletel, Mechanism for Anomalous Hall Ferromagnetism in Twisted Bilayer Graphene, Phys. Rev. Lett. **124**, 166601 (2020).
[35] K. Hejazi, X. Chen, and L. Balents, Hybrid Wannier Chern bands in magic angle twisted bilayer graphene and the quantized anomalous Hall effect, Phys. Rev. Research **3**, 013242 (2021).
[36] D. E. Parker, T. Soejima, J. Hauschild, M. P. Zaletel, and N. Bultinck, Strain-Induced Quantum Phase Transitions in Magic-Angle Graphene, Phys. Rev. Lett. **127**, 027601 (2021).
[37] A. Thomson and J. Alicea, Recovery of massless Dirac fermions at charge neutrality in strongly interacting twisted bilayer graphene with disorder, Phys. Rev. B **103**, 125138 (2021).
[38] M. Christos, S. Sachdev, and M. S. Scheurer, Superconductivity, correlated insulators, and Wess-Zumino-Witten terms in twisted bilayer graphene, Proc. Natl. Acad. Sci. U.S.A. **117**, 29543 (2020).
[39] E. Khalaf, S. Chatterjee, N. Bultinck, M. P. Zaletel, and A. Vishwanath, Charged skyrmions and topological origin of superconductivity in magic-angle graphene, Sci. Adv. **7**, eabf5299 (2021).
[40] S. Chatterjee, M. Ippoliti, and M. P. Zaletel, Skyrmion Superconductivity: DMRG evidence for a topological route to superconductivity, arXiv:2010.01144.
[41] T. Cea, P. A. Pantalen, N. R. Walet, and F. Guinea, Electrostatic interactions in twisted bilayer graphene, arXiv:2109.06038.
[42] J. M. Park, Y. Cao, K. Watanabe, T. Taniguchi, and P. Jarillo-Herrero, Flavour hunds coupling, chern gaps and charge diffusivity in moir graphene, Nature (London) **592**, 4348 (2021).
[43] Y. Cao, D. Rodan-Legrain, J. M. Park, N. F. Q. Yuan, K. Watanabe, T. Taniguchi, R. M. Fernandes, L. Fu, and P. Jarillo-Herrero, Nematicity and competing orders in superconducting magic-angle graphene, Science **372**, 264271 (2021).
[44] X. Liu, Z. Wang, K. Watanabe, T. Taniguchi, O. Vafek, and J. Li, Tuning electron correlation in magic-angle twisted bilayer graphene using coulomb screening, Science **371**, 1261 (2021).
[45] U. Zondiner, A. Rozen, D. Rodan-Legrain, Y. Cao, R. Queiroz, T. Taniguchi, K. Watanabe, Y. Oreg, F. von Oppen, A. Stern *et al.*, Cascade of phase transitions and Dirac revivals in magic-angle graphene, Nature (London) **582**, 203 (2020).
[46] A. Uri, S. Grover, Y. Cao, J. A. Crosse, K. Bagani, D. Rodan-Legrain, Y. Myasoedov, K. Watanabe, T. Taniguchi, P. Moon *et al.*, Mapping the twist-angle disorder and landau levels in magic-angle graphene, Nature (London) **581**, 47 (2020).
[47] Y. Saito, J. Ge, K. Watanabe, T. Taniguchi, and A. F. Young, Independent superconductors and correlated insulators in twisted bilayer graphene, Nat. Phys. **16**, 926 (2020).
[48] I. Das, X. Lu, J. Herzog-Arbeitman, Z.-D. Song, K. Watanabe, T. Taniguchi, B. A. Bernevig, and D. K. Efetov, Symmetry-broken Chern insulators and Rashba-like landau-level crossings in magic-angle bilayer graphene, Nat. Phys. **17**, 710 (2021).
[49] Y. Saito, F. Yang, J. Ge, X. Liu, T. Taniguchi, K. Watanabe, J. Li, E. Berg, and A. F. Young, Isospin Pomeranchuk effect in twisted bilayer graphene, Nature (London) **592**, 220 (2021).
[50] A. Rozen, J. M. Park, U. Zondiner, Y. Cao, D. Rodan-Legrain, T. Taniguchi, K. Watanabe, Y. Oreg, A. Stern, E. Berg *et al.*, Entropic evidence for a Pomeranchuk effect in magic-angle graphene, Nature (London) **592**, 214 (2021).
[51] P. Stepanov, I. Das, X. Lu, A. Fahimniya, K. Watanabe, T. Taniguchi, F. H. L. Koppens, J. Lischner, L. Levitov, and D. K. Efetov, Untying the insulating and superconducting orders in magic-angle graphene, Nature (London) **583**, 375 (2020).
[52] S. Wu, Z. Zhang, K. Watanabe, T. Taniguchi, and E. Y. Andrei, Chern insulators, van Hove singularities and topological flat bands in magic-angle twisted bilayer graphene, Nat. Mater. **20**, 488494 (2021).
[53] A. T. Pierce, Y. Xie, J. M. Park, E. Khalaf, S. H. Lee, Y. Cao, D. E. Parker, P. R. Forrester, S. Chen, K. Watanabe,

T. Taniguchi, A. Vishwanath, P. Jarillo-Herrero, and A. Yacoby, Unconventional sequence of correlated Chern insulators in magic-angle twisted bilayer graphene, Nat. Phys. **17**, 1210 (2021).

[54] H. Polshyn, M. Yankowitz, S. Chen, Y. Zhang, K. Watanabe, T. Taniguchi, C. R. Dean, and A. F. Young, Large linear-in-temperature resistivity in twisted bilayer graphene, Nat. Phys. **15**, 1011 (2019).

[55] P. Stepanov, M. Xie, T. Taniguchi, K. Watanabe, X. Lu, A. H. MacDonald, B. A. Bernevig, and D. K. Efetov, Competing Zero-Field Chern Insulators in Superconducting Twisted Bilayer Graphene, Phys. Rev. Lett. **127**, 197701 (2021).

[56] A. Kerelsky, L. J. McGilly, D. M. Kennes, L. Xian, M. Yankowitz, S. Chen, K. Watanabe, T. Taniguchi, J. Hone, C. Dean *et al.*, Maximized electron interactions at the magic angle in twisted bilayer graphene, Nature (London) **572**, 95 (2019).

[57] Y. Choi, J. Kemmer, Y. Peng, A. Thomson, H. Arora, R. Polski, Y. Zhang, H. Ren, J. Alicea, G. Refael *et al.*, Electronic correlations in twisted bilayer graphene near the magic angle, Nat. Phys. **15**, 1174 (2019).

[58] Y. Xie, B. Lian, B. Jäck, X. Liu, C.-L. Chiu, K. Watanabe, T. Taniguchi, B. A. Bernevig, and A. Yazdani, Spectroscopic signatures of many-body correlations in magic angle twisted bilayer graphene, Nature (London) **572**, 101 (2019).

[59] D. Wong, K. P. Nuckolls, M. Oh, B. Lian, Y. Xie, S. Jeon, K. Watanabe, T. Taniguchi, B. A. Bernevig, and A. Yazdani, Cascade of electronic transitions in magic-angle twisted bilayer graphene, Nature (London) **582**, 198 (2020).

[60] Y. Choi, H. Kim, Y. Peng, A. Thomson, C. Lewandowski, R. Polski, Y. Zhang, H. S. Arora, K. Watanabe, T. Taniguchi *et al.*, Correlation-driven topological phases in magic-angle twisted bilayer graphene, Nature (London) **589**, 536 (2021).

[61] Y. Choi, H. Kim, C. Lewandowski, Y. Peng, A. Thomson, R. Polski, Y. Zhang, K. Watanabe, T. Taniguchi, J. Alicea, and S. Nadj-Perge, Interaction-driven band flattening and correlated phases in twisted bilayer graphene, arXiv: 2102.02209.

[62] S. L. Tomarken, Y. Cao, A. Demir, K. Watanabe, T. Taniguchi, P. Jarillo-Herrero, and R. C. Ashoori, Electronic Compressibility of Magic-Angle Graphene Superlattices, Phys. Rev. Lett. **123**, 046601 (2019).

[63] J. Yu, B. A. Foutty, Z. Han, M. E. Barber, Y. Schattner, K. Watanabe, T. Taniguchi, P. Phillips, Z.-X. Shen, S. A. Kivelson, and B. E. Feldman, Correlated hofstadter spectrum and flavor phase diagram in magic angle graphene, arXiv:2108.00009.

[64] Y. Saito, J. Ge, L. Rademaker, K. Watanabe, T. Taniguchi, D. A. Abanin, and A. F. Young, Hofstadter subband ferromagnetism and symmetry-broken chern insulators in twisted bilayer graphene, Nat. Phys. **17**, 478 (2021).

[65] See Supplemental Material at http://link.aps.org/supplemental/10.1103/PhysRevLett.128.156401, which contains Ref. [66], for figures of several other order parameters in addition to the ones shown in the main text, a detailed discussion of the Landau fans, and finite temperature HF results.

[66] B. A. Bernevig, Z.-D. Song, N. Regnault, and B. Lian, Twisted bilayer graphene. III. Interacting Hamiltonian and exact symmetries, Phys. Rev. B **103**, 205413 (2021).

[67] Y.-H. Zhang, H. C. Po, and T. Senthil, Landau level degeneracy in twisted bilayer graphene: Role of symmetry breaking, Phys. Rev. B **100**, 125104 (2019).

[68] F. Guinea and N. R. Walet, Electrostatic effects, band distortions, and superconductivity in twisted graphene bilayers, Proc. Natl. Acad. Sci. U.S.A. **115**, 13174 (2018).

[69] L. Rademaker, D. A. Abanin, and P. Mellado, Charge smoothening and band flattening due to Hartree corrections in twisted bilayer graphene, Phys. Rev. B **100**, 205114 (2019).

[70] T. Cea, N. R. Walet, and F. Guinea, Electronic band structure and pinning of fermi energy to van Hove singularities in twisted bilayer graphene: A self-consistent approach, Phys. Rev. B **100**, 205113 (2019).

[71] Z. A. H. Goodwin, V. Vitale, X. Liang, A. A. Mostofi, and J. Lischner, Hartree theory calculations of quasiparticle properties in twisted bilayer graphene, arXiv:2004.14784.

[72] J. Kang, B. A. Bernevig, and O. Vafek, Cascades Between Light and Heavy Fermions in the Normal State of Magic Angle Twisted Bilayer Graphene, Phys. Rev. Lett. **127**, 266402 (2021).

[73] Z. Bi, N. F. Q. Yuan, and L. Fu, Designing flat bands by strain, Phys. Rev. B **100**, 035448 (2019).

[74] We term this a spin-Hall state since opposite spins have opposite Chern number, leading to a spin Hall current. However this state is *not* a topological insulator and does not have spin-Kramers time reversal symmetry.